Original Paper

Ophthalmologica

Ophthalmologica
DOI: 10.1159/000456083

Received: July 24, 2016
Accepted after revision: January 13, 2017
Published online: February 8, 2017

Comparison of 55° Wide-Field Spectral Domain Optical Coherence Tomography and Conventional 30° Optical Coherence Tomography for the Assessment of Diabetic Macular Edema

Marion R. Munk[a, b] Joel Lincke[a] Helena Giannakaki-Zimmermann[a, b]
Andreas Ebneter[a, c] Sebastian Wolf[a, b, c] Martin S. Zinkernagel[a, b, c]

[a]Department of Ophthalmology, Inselspital, University Clinic Bern, [b]Bern Photographic Reading Center, University Clinic Bern, and [c]Department of Clinical Research, Inselspital, University Clinic Bern, Bern, Switzerland

Keywords
Wide-field imaging · Diabetic macular edema · Wide-field spectral domain optical coherence tomography · Microaneurysms · Vitreoretinal interface · Macular edema · Subretinal fluid · Intraretinal fluid · Hard exudates

Abstract

Purpose: To compare conventional 30° spectral domain optical coherence tomography (SD-OCT) with 55° wide-field SD-OCT for the assessment of diabetic macular edema (DME). ***Methods:*** This study included 50 DME patients. Both 55° and 30° SD-OCT was conducted. Two readers evaluated scans according to a standardized grading protocol. Intergrader agreement as well as agreement between 30° and 55° SD-OCT were assessed. ***Results:*** Intergrader agreement (κ) was strong and ranged from 0.79 to 1.0. Perfect interdevice agreement (κ = 1.0) was found for the detection of intra- and subretinal fluid. Excellent agreement (κ ≥ 0.9) was found for the presence of epiretinal membrane (κ = 0.92) and cotton-wool spots (κ = 0.92). A strong agreement was found for the presence of hard exudates (κ = 0.89) and microaneurysms (κ = 0.81). A moderate correlation was found for ellipsoid zone integrity (κ = 0.69) and configuration of the vitreomacular interface (VMI) (κ = 0.69). A weak agreement was found for retinal pigment epithelium atrophy (κ = 0.51) and external limiting membrane integrity (κ = 0.35). ***Conclusion:*** Wide-field OCT imaging may be beneficial for evaluating DME, particularly for assessing the VMI and the integrity of hyperreflective bands.

Introduction

Optical coherence tomography (OCT) allows for high-resolution cross-sectional imaging of tissue in a noninvasive fashion by reflected light [1]. It is used to diagnose various ophthalmologic pathologies [2]. One of its applications is the screening and sequential monitoring of patients with diabetic macular edema (DME), whereby the respective macular thickness, the presence of intraretinal and subretinal fluid (SRF), as well as typical morphological features such as microaneurysms (MA), hard exudates (HE), and the integrity of the reti-

KARGER

E-Mail karger@karger.com
www.karger.com/oph

0030–3755/17/0000–0000$39.50/0

Marion R. Munk, MD, PhD
Inselspital, University Clinic Bern
Freiburgerstrasse 4
CH–3010 Bern (Switzerland)
E-Mail marion_munk@hotmail.com

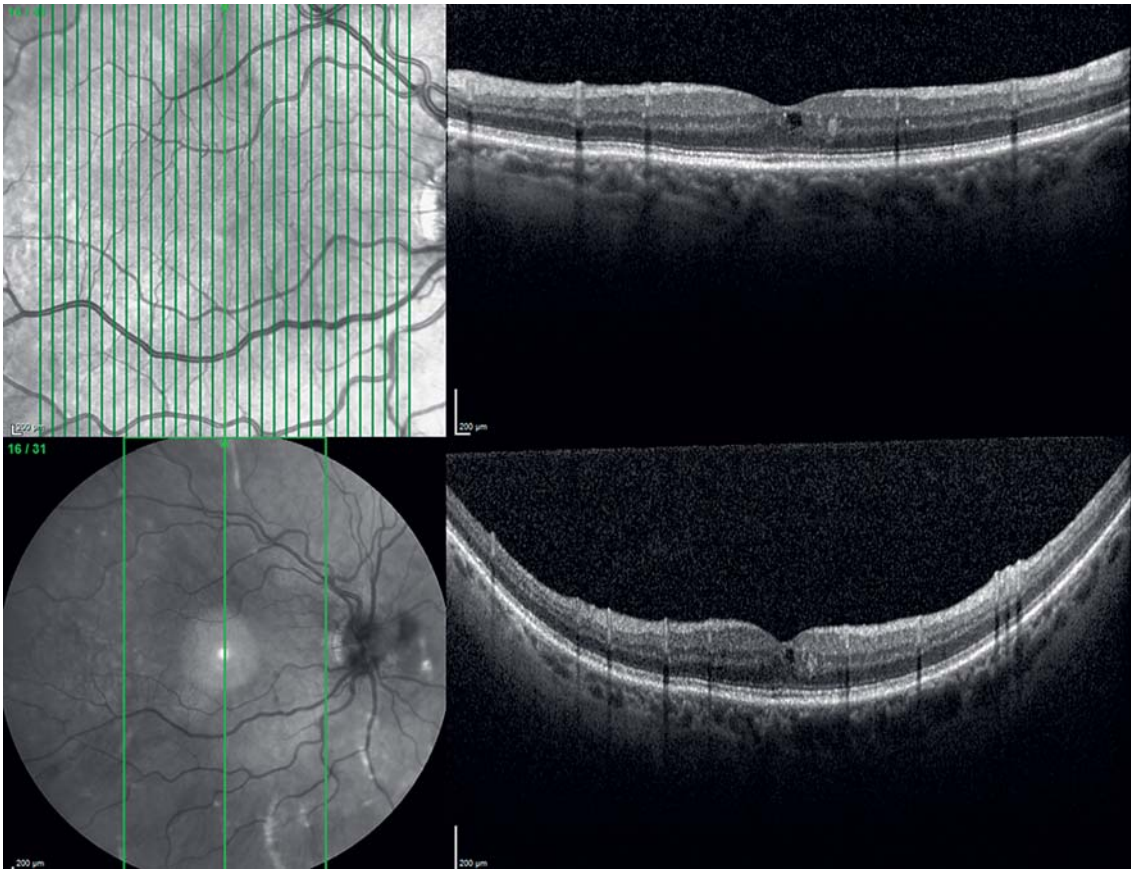

Fig. 1. Representative example of DME assessed with conventional 30° SD-OCT (top) and 55° wide-field SD-OCT (bottom).

nal pigment epithelium (RPE) and the photoreceptor layers can be quantified [3, 4]. The technology of OCT has been steadily improved. One of the advancements is the widening of the scanning angle, with modern technology being able of process up to 100° in a single image [5]. This allows a greater area of the retina to be imaged and thus examined at once, which could potentially be of great benefit for the diagnosis, treatment decision, and even understanding of the pathophysiology leading to retinal diseases [6]. Several wide-field OCT systems have been developed using e.g. extended-field imaging or imaging montage [7–11].

For the monitoring of DME patients during treatment, standard 30° spectral domain OCT (SD-OCT) is commonly used, but with wide-field SD-OCT becoming commercially available, we wanted to examine whether 55° wide-field SD-OCT is superior compared to regular 30° SD-OCT imaging for the diagnostic assessment of DME.

Methods

Patients and Setting

The study adhered to the tenets of the Declaration of Helsinki and was approved by the local ethics committee at Inselspital. This cross-sectional study included Spectralis 55° wide-field and conventional 30° SD-OCT of the eyes of participants with DME.

Conventional and wide-field SD-OCTs of 50 consecutive patients from the Outpatient Clinics of the Department for Ophthalmology, Inselspital, University Clinic Bern with a diagnosis of DME were retrospectively assessed. All SD-OCT images were acquired using the Spectralis SD-OCT (Heidelberg Engineering, Germany) system (Heidelberg Eye Explorer 1.9.10.0) and were scanned using the 55° wide-field SD-OCT module consisting of a 55° wide-field lens and a dedicated software as well as the regular Heidelberg 30° lens on the same day. The 55° high-speed wide-field volume scan pattern included a 55° × 25° vertical raster scan pattern consisting of 31 section scans (distance between scans 240 µm), with each scan 9 times averaged. The corresponding 30° high-speed volume scan pattern consisted of a 30° × 25° vertical raster scan with 31 section scans (distance between scans 240 µm), each scan 9 times averaged. Hence, the horizontal area scanned as well as the distance between the scans

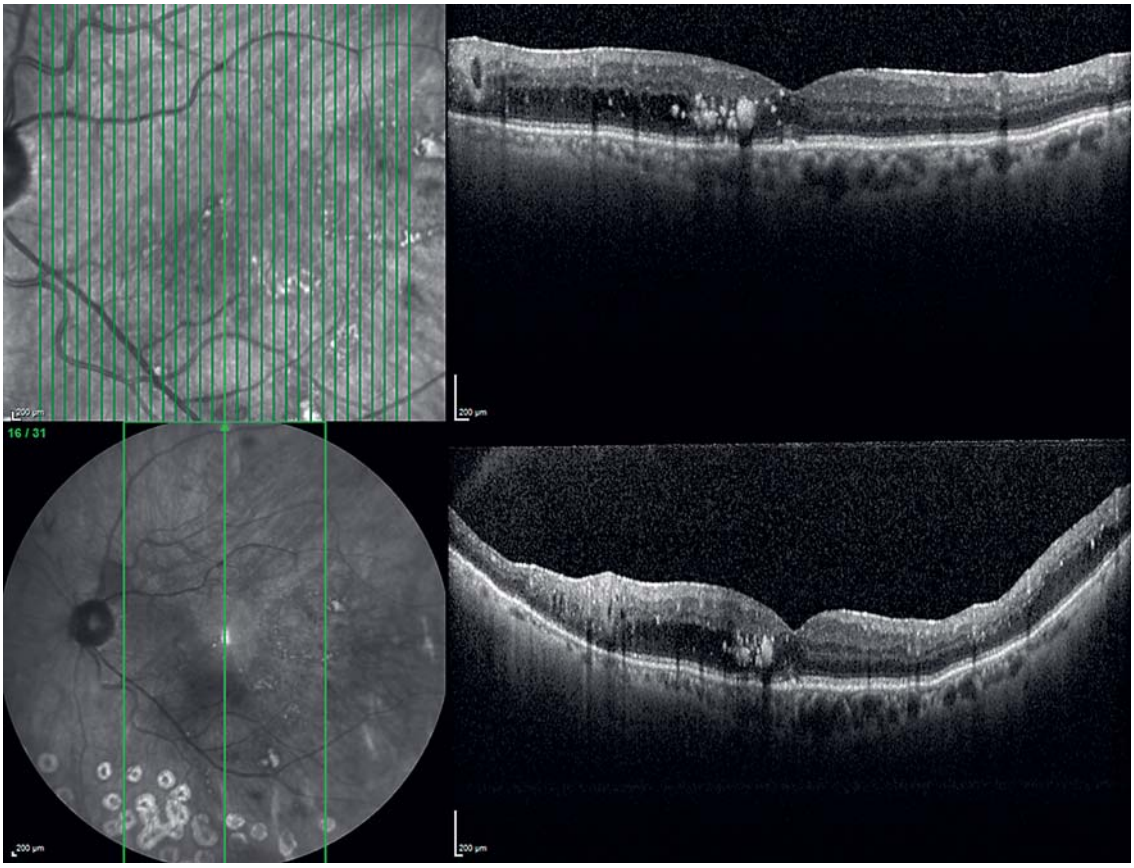

Fig. 2. Representative example of DME assessed with conventional 30° SD-OCT (top) and 55° wide-field SD-OCT (bottom).

were equal, and only the vertical extension of the scans (30° vs. 55°) differed between both scan patterns. As the integrated follow-up mode on conventional OCT does not allow the acquisition of 55° OCT using the respective follow-up function, the authors payed particular attention to the location of the scans in order to allow accurate scan by scan comparison. Two representative images for the 30° and 55° wide-field SD-OCT are shown in Figures 1 and 2. Only high-quality, well-resolved raster scans with a minimum of 20 dB signal-to-noise ratio were included for analysis [12].

The volume scans including all 31 images were analyzed according to a standardized grading protocol, which included presence of SRF, intraretinal fluid (IRF)/cystoid macular edema (CME) in the outer nuclear layer (ONL), inner nuclear layer (INL), ganglion cell layer (GCL) and retinal nerve fiber layer (RNFL), presence of epiretinal membrane (ERM), integrity of the external limiting membrane (ELM), the ellipsoid zone (EZ) and the RPE, presence of HE, MA and cotton-wool spots (CWS), and configuration of the vitreomacular interface (VMI). The height of SRF and the cyst area were evaluated in the central line scan. SRF was defined as a hyporeflective area between the RPE and the photoreceptor layer >100 µm in horizontal direction [13]. CME was defined as round or oval areas of low reflectivity with a minimum size of 25 µm in any direction [14]. ERM was

Table 1. Intergrader agreement of evaluated 30° and 55° SD-OCT parameters

Morphological features	Kappa 55°	Kappa 30°
Subretinal fluid	0.85	0.85
Intraretinal fluid	1.0	1.0
Intraretinal fluid ONL	0.93	1.0
Intraretinal fluid INL	0.91	1.0
Intraretinal fluid GCL	0.96	0.96
Intraretinal fluid RNFL	0.94	1.0
Epiretinal membrane	0.96	0.92
ELM integrity	1.0	0.88
Ellipsoid zone integrity	1.0	0.92
RPE integrity	1.0	0.92
Hard exudates	0.92	0.89
Microaneurysms	0.81	0.85
Cotton-wool spots	0.96	1.0
Vitreomacular interface	0.79	0.85

ELM, external limiting membrane; GCL, ganglion cell layer; INL, inner nuclear layer; ONL, outer nuclear layer; RNFL, retinal nerve fiber layer; RPE, retinal pigment epithelium; SD-OCT, spectral domain optical coherence tomography.

Table 2. Concordance of findings between conventional 30° and 55° wide-field SD-OCT

Morphological features	Presence 30°, *n* (%)	Presence 55°, *n* (%)	Kappa	*p* value
Subretinal fluid	4 (8%)	4 (8%)	1.0	<0.0001
Intraretinal fluid	46 (92%)	46 (92%)	1.0	<0.0001
Intraretinal fluid ONL	41 (82%)	42 (84%)	0.93	<0.0001
Intraretinal fluid INL	43 (86%)	44 (88%)	0.91	<0.0001
Intraretinal fluid GCL	23 (46%)	25 (50%)	0.84	<0.0001
Intraretinal fluid RNFL	8 (16%)	11 (22%)	0.81	<0.0001
Epiretinal membrane	26 (52%)	26 (52%)	0.92	<0.0001
ELM integrity	20 (40%)	8 (16%)	0.35	0.003
Ellipsoid zone integrity	20 (40%)	13 (26%)	0.69	<0.0001
RPE atrophy	21 (42%)	34 (68%)	0.51	<0.0001
Hard exudates	45 (90%)	44 (88%)	0.89	<0.0001
Microaneurysms	43 (86%)	45 (90%)	0.81	<0.0001
Cotton-wool spots	0 (0%)	1 (2%)	0.92	<0.0001
Vitreomacular interface			0.69	<0.0001
Complete PVD	13 (26%)	11 (22%)		
Incomplete PVD	7 (14%)	7 (14%)		
VMA	4 (8%)	8 (16%)		
PVA	26 (52%)	24 (48%)		
Quantitative parameters (mean ± SD)			*R*	*p* value
Subretinal fluid height	40±10.5 μm	40.3±10.1 μm	0.99	0.021
Cyst area	0.058±0.05 mm^2	0.06±0.05 mm^2	0.89	<0.0001
Number of microaneurysms	2.44±2.3	2.46±2.2	0.88	<0.0001

Parameters with weaker agreement are highlighted in grey. ELM, external limiting membrane; GCL, ganglion cell layer; INL, inner nuclear layer; ONL, outer nuclear layer; PVA, posterior vitreous attachment; PVD, posterior vitreous detachment; RNFL, retinal nerve fiber layer; RPE, retinal pigment epithelium; SD-OCT, spectral domain optical coherence tomography; VMA, vitreomacular adhesion.

defined as a hyperreflective band attached to the internal limiting membrane [15]. HE were defined as irregular intraretinal accumulations of hyperreflective material with a typical shadowing below [16]. MA were defined as oval and well-demarcated intraretinal ring-like lesions [14]. CWS were defined as homogenous localized lesions of intensive hyperreflectivity at the level of the RNFL associated with light attenuation below [16]. The VMI was classified as complete posterior vitreous detachment (PVD), incomplete PVD, vitreomacular traction, vitreomacular adhesion, or posterior vitreous attachment. Complete PVD was graded as present when the vitreous boundary was not visible at all on any SD-OCT scan [17]. Incomplete PVD was present if the preretinal hyperreflective band was visible above the SD-OCT scan with no contact to the macula [17]. Vitreomacular traction was graded when the preretinal vitreous boundary induced macular traction and caused foveal distortion [17]. Vitreomacular adhesion was present if the hyperreflective vitreous layer was still in contact with the central macula (≤4,000 μm in diameter), but was detached at the borders of the scans without leading to macular traction [17]. Posterior vitreous attachment was present if the vitreomacular adhesion was >4,000 μm in diameter or the vitreous boundary was in continuous contact with the macula [17].

For CME, graders marked the area of the central cyst with the greatest extent on the central foveal scan using the measuring tool of the Heidelberg software. Two independent, experienced graders from the Bern Photographic Reading Center (M.R.M., H.G.-Z.) assessed and graded the images based on the predefined grading protocol. After reader agreement analyses, grading discrepancies were resolved by a reader consensus grading of both graders.

Statistical Analyses

Statistical analyses were performed with the SPSS (IBM, SPSS Statistics, Version 21, SPSS Inc., Chicago, IL, USA) software. Cohen's κ coefficient was employed to quantify intergrader agreement. After concordance analyses, a consensus grading was performed, and the respective consensus datasets of the 30° and 55° SD-OCT were then compared using Cohen's κ in order to evaluate the concordance between the conventional and the wide-field SD-OCT. For congruence in numerical data, Pearson correlation between the measurements on the conventional and wide-field images was obtained. p values <0.05 were considered statistically significant. Values are given as mean ± standard deviation.

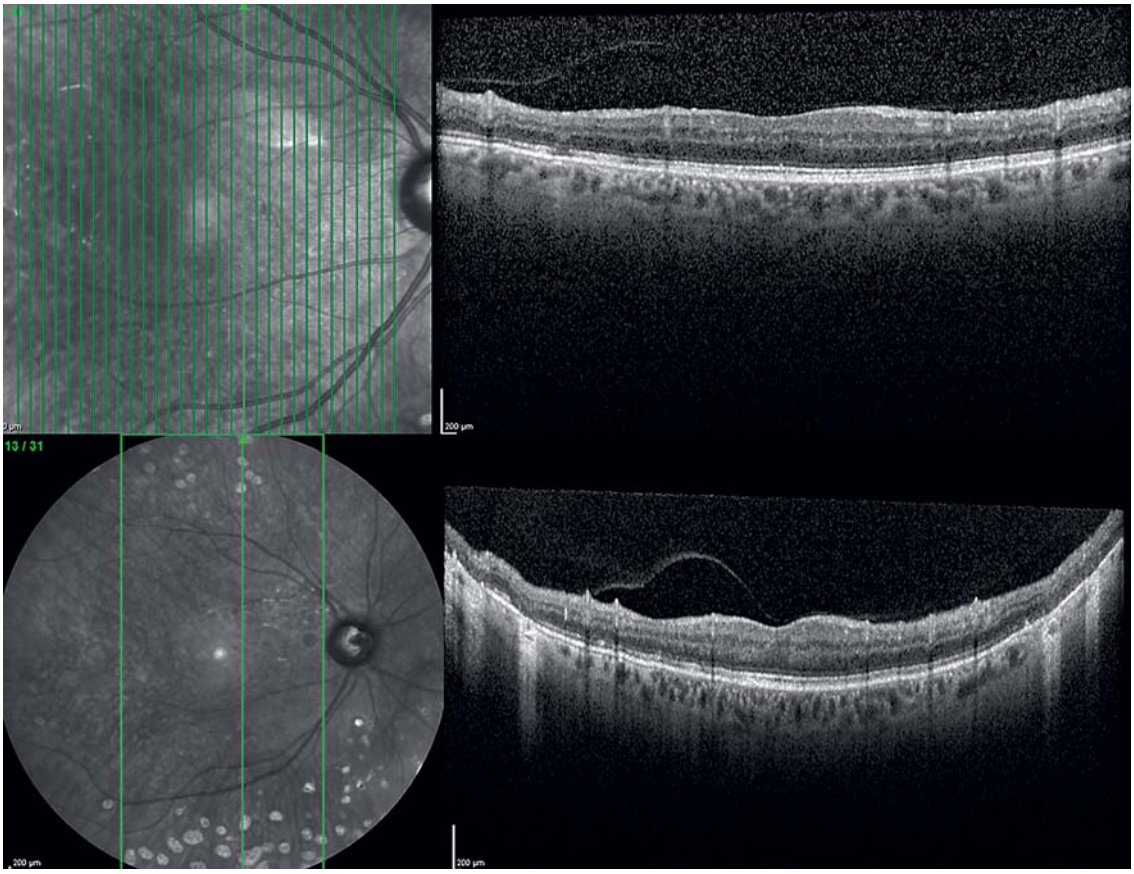

Fig. 3. Representative example of a patient with RPE atrophy due to laser scars on 55° OCT (bottom), which were not apparent on conventional 30° OCT (top).

Results

This study assessed 56 eyes. Six eyes were excluded due to poor image quality, thus 50 eyes of 50 patients (mean age 50 ± 26 years) suffering from DME and receiving continuous intravitreal injections with ranibizumab or aflibercept were included. Intergrader agreement (κ) of selected anatomical features ranged between 0.79 and 1.0. Details can be found in Table 1.

Agreement between Conventional and Wide-Field OCT

A perfect agreement was found in terms of detection of IRF/CME and SRF (κ = 1.0). An excellent agreement (κ ≥ 0.9) was found for the presence of IRF in the ONL or INL, the presence of an ERM, and the presence of CWS. A strong agreement (κ = 0.8–0.9) was found for the presence of IRF within the GCL and the RNFL as well as the presence of HE and MA. A moderate agreement (κ = 0.6–0.79) was found for the integrity of the EZ and the configuration of the VMI. A weak agreement was found in terms of RPE atrophy (κ = 0.51), and minimal agreement was found for ELM integrity (κ = 0.35) [18]. Detailed information on the level of agreement of each evaluated parameter can be found in Table 2. Cross tables for the variables VMI, RPE, EZ, and ELM integrity, which showed rather a weak agreement, can be found in online supplementary Tables 1–4 (for all online suppl. material, see www.karger.com/doi/10.1159/000456083).

In cases of disagreement between conventional 30° and 55° wide-field SD-OCT, alterations were usually detected on the 55° and missed on the 30° SD-OCT scans due to the greater extent of the 55° scan (Table 2; Fig. 3). However, in some cases alterations were found on 30° but not on 55° SD-OCT: HE were seen in 1 patient on the 30° SD-OCT but were missed on the 55° SD-OCT (Fig. 4). In 1 eye, ELM disruption was found on the 30° scans but was missed on the 55° scan, whereas in 13 cases, ELM disruption was found on the 55° wide-field scans, with an intact ELM seen on the 30° scans. ERM was detected in 1 patient on the 30° scan, but was missed on the wide-field SD-

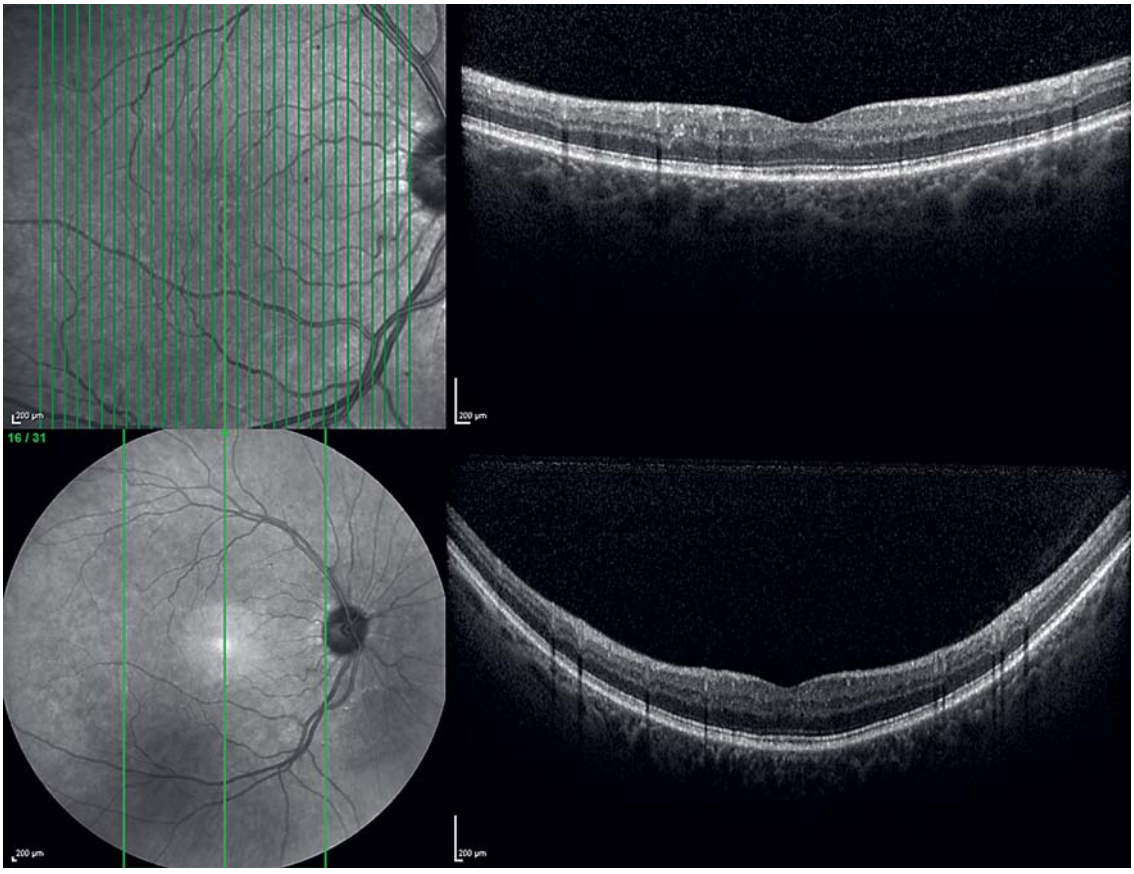

Fig. 4. Hard exudates were found on conventional 30° OCT (top), which were missed on 55° OCT (bottom).

OCT, whereas another patient showed an ERM on the 55° scan, which was not found on the conventional SD-OCT. GCL cysts were discovered in 1 patient on 30° scans and missed on 55° scans, whereas 3 patients had GCL cysts on 55° SD-OCT which were not seen on 30° SD-OCT. Thus, in 4 cases disagreement was due to the fact that alterations were found on 30° OCT, but were missed on 55° SD-OCT. The remaining discrepancy was due to the greater field of view on 55° SD-OCT, and alterations were detected on the 55° and missed on the 30° SD-OCT scans.

Subanalysis according to the Presence of Panretinal Photocoagulation

Twenty-six eyes (52%) had panretinal photocoagulation (PRP) laser scars. One eye (2%) had focal laser scars in the macula. The subgroup with PRP laser scars showed minimal agreement in respect to the integrity of the RPE ($\kappa = 0.15$, $p = 0.1$), the EZ ($\kappa = 0.17$, $p = 0.09$), and the ELM ($\kappa = 0$, $p = 1$). In contrast, the group without prior PRP laser treatment presented strong agreement among these features (RPE integrity: $\kappa = 0.82$, $p \leq 0.001$; EZ integrity: $\kappa = 0.92$, $p \leq 0.001$; ELM integrity: $\kappa = 0.5$, $p = 0.009$). Cross tables of respective parameters can be found in supplementary Tables 1–3.

Discussion

Wide-field images including color fundus imaging, fluorescein angiography, and fundus autofluorescence are currently being introduced into clinical practice and are of particular interest to explore peripheral changes associated with various diseases such as diabetic retinopathy and uveitis, but also age-related macular degeneration. Wide-field OCT is a new method and of great interest especially when both the periphery as well as the posterior pole need to be assessed in a single scan [11]. So far, wide-field and ultra-wide-field OCT were used in order to describe the peripheral retinochoroid morphology and peripheral changes associated with retinitis pigmentosa, choroidal nevi, choroidal melanomas, acute exudative polymorphous vitelliform maculopathy, macular holes,

and congenital X-linked retinoschisis [6, 8, 10, 11, 19, 20]. This is the first study to compare conventional 30° with 55° wide-field SD-OCT using a predefined scanning pattern and grading protocol in order to assess whether wide-field SD-OCT may also offer potential benefit in diseases mainly confined to the macular area, and whether it may allow a more precise detection of morphological features outside conventional 30° OCT. We found a strong agreement between both image modalities for morphological features such as IRF, SRF, HE, CWS, and MA. The agreement for the configuration of VMI, ELM, and RPE integrity however was only moderate to weak. This implicates that 55° SD-OCT may provide additional information also in diseases mainly restricted to the posterior pole.

The VMI was one morphological feature with only a moderate agreement between both images. These discrepancies can possibly be explained by the greater scanning angle of 55° that allows the visualization of a larger retinal area and therefore a more precise evaluation of the VMI. Correct assessment of the VMI is of particular interest, given that the configuration impacts the treatment response and treatment need in DME, but also in exudative age-related macular degeneration and CME due to uveitis or retinal vein occlusions [17, 21, 22]. Wide-field OCT studies showed that the vitreous interface can be clearly delineated using this imaging technique [8, 10, 19]. These findings emphasize the critical role of the correct assessment of the vitreous cortex in respective diseases, which may be facilitated using wide-field SD-OCT.

Beside the VMI, there was also only a moderate to weak agreement in terms of ELM and RPE integrity. This is easily explained by the subgroup analysis in respect to prior PRP treatment: eyes without PRP laser scars showed a strong agreement in respective parameters, whereas eyes with PRP laser scars had only a weak agreement. In conventional 30° SD-OCT, these laser burns with associated loss of the photoreceptor layer and RPE atrophy will not be identifiable; however, using a wide-field scan which extends beyond the vascular arcades allows the depiction of respective laser burns on SD-OCT.

Although most of the discrepancies between 30° and 55° SD-OCT were due to the fact that additional alterations outside of the 30° range were found on 55° OCT, some discrepancies originated from the fact that features were missed on 55° OCT, but were identifiable on 30° SD-OCT. The higher resolution on the 30° images may be the underlying reason for these findings. Conventional 30° as well as 55° wide-field images were attained in high-speed mode, which resulted in a resolution of 768 pixels on the *x* axis and 496 pixels on the *z* axis. This resulted in a higher horizontal resolution of 11.74 μm/pixel in the conventional OCT scans compared to 19.95 μm/pixel in the wide-field scans, which may explain that in some cases, morphological alterations such as HE were missed on the 55° image. Another explanation may be the fact that although in both scans a horizontal area of 25° was imaged with particular attention to the best possible alignment of each scan of both raster scans, the single scans were not always on the exact same location [23]. This may have led to the presence of respective alterations on one scan but absence on the other scan and should be considered as a limitation of this study.

Although the concordance for the overall presence of IRF was 1.0, in some patients additional peripheral IRF in the INL, GCL, and RNFL was identified on the wide-field SD-OCT. The question whether these additional findings would change the treatment regimen in these patients and/or involve different treatment approaches goes beyond the focus of this paper. Whether the identification of additional extrafoveal IRF may require additional focal/grid laser because of the extrafoveal location of the macular edema or anti-VEGF treatment may be individually discussed. One may also argue that there is no need of additional treatment due to the extrafoveal location of the IRF. According to the American Academy of Ophthalmology preferred practice patterns, the treatment of choice in center-involving DME is anti-VEGF therapy with possible subsequent or deferred laser treatment [24]. Non-center-involving DME should be treated with focal/grid laser [24, 25]. Whether the identification of additional IRF beyond the central 30° would result in additional treatment and whether patients would really benefit from additional treatment remains elusive based on our data, and future studies are warranted in order to explore the benefit of wide-field OCT to optimize treatment decisions for macular diseases.

The limitations of this study include the fact that the scans of the conventional and the wide-field SD-OCTs were aligned manually due to lack of a rescanning feature between the two lenses. As such, there may have been some degree of misalignment.

In conclusion, we here compare for the first time conventional 30° SD-OCT with 55° wide-field SD-OCT in DME. Further studies are warranted to delineate the potential role of wide-field SD-OCT imaging in daily clinic and in the management of macular diseases such as DME and exudative age-related macular degeneration. In particular, prospective studies are needed in order to explore the benefit of wide-field OCT in the treatment decision-making for macular diseases.

Acknowledgments

Marion R. Munk received lecturer fees from Novartis AG and travel support from Bayer AG and is a consultant for Lumithera. Andreas Ebneter received lecturer fees and travel support from Bayer AG. Sebastian Wolf is consultant for Bayer and Novartis, and Martin Zinkernagel is consultant for Novartis and Bayer AG. Joel Lincke and Helena Giannakaki-Zimmermann have no financial relations to disclose.

Disclosure Statement

The authors have no conflict of interest to report. They have no commercial or proprietary interest in the content of this paper and received no funding or financial support for this study.

References

1 Huang D, Swanson EA, Lin CP, Schuman JS, Stinson WG, Chang W, Hee MR, Flotte T, Gregory K, Puliafito CA, et al: Optical coherence tomography. Science 1991;254:1178–1181.
2 Zysk AM, Nguyen FT, Oldenburg AL, Marks DL, Boppart SA: Optical coherence tomography: a review of clinical development from bench to bedside. J Biomed Opt 2007;12:051403.
3 Hee MR, Puliafito CA, Duker JS, Reichel E, Coker JG, Wilkins JR, Schuman JS, Swanson EA, Fujimoto JG: Topography of diabetic macular edema with optical coherence tomography. Ophthalmology 1998;105:360–370.
4 Browning DJ, McOwen MD, Bowen RM Jr, O'Marah TL: Comparison of the clinical diagnosis of diabetic macular edema with diagnosis by optical coherence tomography. Ophthalmology 2004;111:712–715.
5 Kolb JP, Klein T, Kufner CL, Wieser W, Neubauer AS, Huber R: Ultra-widefield retinal MHz-OCT imaging with up to 100 degrees viewing angle. Biomed Opt Express 2015;6:1534–1552.
6 Carrai P, Pichi F, Bonsignore F, Ciardella AP, Nucci P: Wide-field spectral domain-optical coherence tomography in central serous chorioretinopathy. Int Ophthalmol 2015;35:167–171.
7 Uji A, Yoshimura N: Application of extended field imaging to optical coherence tomography. Ophthalmology 2015;122:1272–1274.
8 Pichi F, Carrai P, Bonsignore F, Villani E, Ciardella AP, Nucci P: Wide-field spectral domain optical coherence tomography. Retina 2015;35:2584–2592.
9 Gregori NZ, Lam BL, Gregori G, Ranganathan S, Stone EM, Morante A, Abukhalil F, Aroucha PR: Wide-field spectral-domain optical coherence tomography in patients and carriers of X-linked retinoschisis. Ophthalmology 2013;120:169–174.
10 Mori K, Kanno J, Gehlbach PL: Retinochoroidal morphology described by wide-field montage imaging of spectral domain optical coherence tomography. Retina 2016;36:375–384.
11 McNabb RP, Grewal DS, Mehta R, Schuman SG, Izatt JA, Mahmoud TH, Jaffe GJ, Mruthyunjaya P, Kuo AN: Wide field of view swept-source optical coherence tomography for peripheral retinal disease. Br J Ophthalmol 2016;100:1377–1382.
12 Balasubramanian M, Bowd C, Vizzeri G, Weinreb RN, Zangwill LM: Effect of image quality on tissue thickness measurements obtained with spectral domain-optical coherence tomography. Opt Express 2009;17:4019–4036.
13 Munk MR, Kiss CG, Huf W, Montuoro A, Sulzbacher F, Kroh M, Larsen M, Schmidt-Erfurth U: Visual acuity and microperimetric mapping of lesion area in eyes with inflammatory cystoid macular oedema. Acta Ophthalmol 2014;92:332–338.
14 Munk MR, Sacu S, Huf W, Sulzbacher F, Mittermuller TJ, Eibenberger K, Rezar S, Bolz M, Kiss CG, Simader C, Schmidt-Erfurth U: Differential diagnosis of macular edema of different pathophysiologic origins by spectral domain optical coherence tomography. Retina 2014;34:2218–2232.
15 Duker JS, Kaiser PK, Binder S, de Smet MD, Gaudric A, Reichel E, Sadda SR, Sebag J, Spaide RF, Stalmans P: The International Vitreomacular Traction Study Group classification of vitreomacular adhesion, traction, and macular hole. Ophthalmology 2013;120:2611–2619.
16 Munk MR, Jampol LM, Simader C, Huf W, Mittermuller TJ, Jaffe GJ, Schmidt-Erfurth U: Differentiation of diabetic macular edema from pseudophakic cystoid macular edema by spectral-domain optical coherence tomography. Invest Ophthalmol Vis Sci 2015;56:6724–6733.
17 Munk MR, Ram R, Rademaker A, Liu D, Setlur V, Chau F, Schmidt-Erfurth U, Goldstein DA: Influence of the vitreomacular interface on the efficacy of intravitreal therapy for uveitis-associated cystoid macular oedema. Acta Ophthalmol 2015;93:e561–e567.
18 McHugh ML: Interrater reliability: the kappa statistic. Biochem Med (Zagreb) 2012;22:276–282.
19 Mori K, Kanno J, Gehlbach PL, Yoneya S: Montage images of spectral-domain optical coherence tomography in eyes with idiopathic macular holes. Ophthalmology 2012;119:2600–2608.
20 Rao P, Robinson J, Yonekawa Y, Thomas BJ, Drenser KA, Trese MT, Capone A Jr: Wide-field imaging of nonexudative and exudative congenital X-linked retinoschisis. Retina 2016;36:1093–1100.
21 Sadiq MA, Soliman MK, Sarwar S, Agarwal A, Hanout M, Demirel S, Rentiya ZS, Khan W, Do DV, Nguyen QD, Sepah YJ: Effect of vitreomacular adhesion on treatment outcomes in the Ranibizumab for Edema of the Macula in Diabetes (READ-3) Study. Ophthalmology 2016;123:324–329.
22 Ciulla TA, Ying GS, Maguire MG, Martin DF, Jaffe GJ, Grunwald JE, Daniel E, Toth CA: Influence of the vitreomacular interface on treatment outcomes in the comparison of age-related macular degeneration treatments trials. Ophthalmology 2015;122:1203–1211.
23 Barteselli G, Bartsch DU, Viola F, Mojana F, Pellegrini M, Hartmann KI, Benatti E, Leicht S, Ratiglia R, Staurenghi G, Weinreb RN, Freeman WR: Accuracy of the Heidelberg Spectralis in the alignment between near-infrared image and tomographic scan in a model eye: a multicenter study. Am J Ophthalmol 2013;156:588–592.
24 Diabetic Retinopathy Clinical Research Network, Elman MJ, Qin H, Aiello LP, Beck RW, Bressler NM, Ferris FL 3rd, Glassman AR, Maturi RK, Melia M: Intravitreal ranibizumab for diabetic macular edema with prompt versus deferred laser treatment: three-year randomized trial results. Ophthalmology 2012;119:2312–2318.
25 American Academy of Ophthalmology: Preferred Practice Patterns. Diabetic Retinopathy PPP-2014. http://www.aao.org/preferred-practice-pattern/diabetic-retinopathy-ppp-2014#top (accessed February 17, 2016).